Radiology

Increased Speed and Image Quality for Pelvic Single-Shot Fast Spin-Echo Imaging with Variable Refocusing Flip Angles and Full-Fourier Acquisition[1]

Andreas M. Loening, MD, PhD
Daniel V. Litwiller, PhD
Manojkumar Saranathan, PhD
Shreyas S. Vasanawala, MD, PhD

Purpose: To assess image quality and speed improvements for single-shot fast spin-echo (SSFSE) with variable refocusing flip angles and full-Fourier acquisition (vrfSSFSE) pelvic imaging via a prospective trial performed in the context of uterine leiomyoma evaluation.

Materials and Methods: Institutional review board approval and informed consent were obtained. vrfSSFSE and conventional SSFSE sagittal and coronal oblique acquisitions were performed in 54 consecutive female patients referred for 3-T magnetic resonance (MR) evaluation of known or suspected uterine leiomyomas. Two radiologists who were blinded to the image acquisition technique semiquantitatively scored images on a scale from -2 to 2 for noise, image contrast, sharpness, artifacts, and perceived ability to evaluate uterine, ovarian, and musculoskeletal structures. The null hypothesis of no significant difference between pulse sequences was assessed with a Wilcoxon signed rank test by using a Holm-Bonferroni correction for multiple comparisons.

Results: Because of reductions in specific absorption rate, vrfSSFSE imaging demonstrated significantly increased speed (more than twofold, $P < .0001$), with mean repetition times compared with conventional SSFSE imaging decreasing from 1358 to 613 msec for sagittal acquisitions and from 1494 to 621 msec for coronal oblique acquisitions. Almost all assessed image quality and perceived diagnostic capability parameters were significantly improved with vrfSSFSE imaging. These improvements included noise, sharpness, and ability to evaluate the junctional zone, myometrium, and musculoskeletal structures for both sagittal acquisitions (mean values of 0.56, 0.63, 0.42, 0.56, and 0.80, respectively; all P values $< .0001$) and coronal oblique acquisitions (mean values of 0.81, 1.09, 0.65, 0.93, and 1.12, respectively; all P values $< .0001$). For evaluation of artifacts, there was an insufficient number of cases with differences to allow statistical testing.

Conclusion: Compared with conventional SSFSE acquisition, vrfSSFSE acquisition increases 3-T imaging speed via reduced specific absorption rate and leads to significant improvements in perceived image quality and perceived diagnostic capability when evaluating pelvic structures.

©RSNA, 2016

Online supplemental material is available for this article.

At present, T2-weighted imaging is the mainstay of most pelvic magnetic resonance (MR) imaging protocols (1,2), with benign and malignant gynecological MR imaging protocols typically consisting of multiple planes of T2-weighted fast spin-echo (FSE) imaging (3,4). FSE, however, requires long acquisition times (generally several minutes), with corresponding sensitivity to motion and prolongation of total examination time. These drawbacks have led to the development of single-shot FSE (SSFSE) imaging, also known as half-Fourier acquisition single-shot turbo spin-echo imaging, which is relatively robust to motion and has greatly decreased acquisition times (5). However, SSFSE imaging has its own drawbacks compared with FSE imaging. SSFSE images have a reduced

signal-to-noise ratio owing to the greatly reduced acquisition time, specific absorption rate (SAR) speed limitations at 3 T due to excessive radiofrequency (RF) energy deposition, and blurring due to T2 decay occurring during the extended refocusing echo train (5,6).

In FSE imaging, the use of variable refocusing flip angles has been extensively studied for two- and three-dimensional FSE pulse sequences (7–12). In contrast to the use of a constant refocusing flip angle, as in conventional SSFSE or FSE imaging, the use of a properly designed variable refocusing flip angle echo train can lead to stabilization of the signal amplitude over the course of the echo train, reducing blurring that would otherwise manifest in the phase-encoding direction. Additionally, the incorporation of lower flip angles at the beginning of the echo train slows the effective rate of T2 relaxation (8,11), allowing image contrast to reflect shorter effective echo times. The overall use of lower flip angles decreases RF deposition, which can decrease SAR-limited acquisition times.

An SSFSE with variable refocusing flip angles and full-Fourier acquisition (vrfSSFSE) pulse sequence has recently been implemented (13) that incorporates a variable refocusing flip angle echo train based on the approach of Busse et al (11,14). This pulse sequence allows for full-Fourier (full k-space coverage) acquisition while still achieving clinically relevant effective echo times, rather than the half-Fourier (partial k-space coverage) acquisition used in conventional SSFSE imaging. Since evaluation of uterine leiomyomas (fibroids) is a relatively large component of our local clinical volume for pelvic imaging, we focused on this specific indication. The purpose of this study was to assess

image quality and speed improvements for vrfSSFSE pelvic imaging via a prospective trial performed in the context of uterine leiomyoma evaluation.

Materials and Methods

SSFSE Pulse Sequence

With the conventional SSFSE pulse sequence, a constant refocusing flip angle of 130° was used. Acquisition was half-Fourier with homodyne reconstruction and linear ordering of phase encodes. Effective echo time was set to 120 msec. Additional imaging parameters are shown in Table 1.

vrfSSFSE Pulse Sequence

The vrfSSFSE pulse sequence was implemented as described previously (13). In brief, the refocusing flip angle approach developed for three-dimensional FSE imaging described by Busse et al (11) was adapted to the case of two-dimensional SSFSE imaging. In

---

Advances in Knowledge

- Implementation of variable refocusing flip angles into single-shot fast spin-echo (SSFSE) pulse sequences results in significant improvements in subjective image quality scores of noise and sharpness (mean scores of 0.56 and 0.63 on a −2 to 2 scale for sagittal acquisitions and 0.81 and 1.09 for coronal oblique acquisitions, respectively; all P values < .0001) due to reductions in T2 decay–related blurring, as well as the ability to acquire full-Fourier data with clinically relevant echo times.

- Image acquisition time at 3 T for a series of SSFSE sections can be reduced by more than 50% ($P <$ .0001, mean repetition times decreasing from 1358 to 613 msec for sagittal acquisitions and from 1494 to 621 msec for coronal oblique acquisitions); this arises from the reduced refocusing flip angles decreasing the level of radiofrequency energy deposition, with resultant removal of delays in imaging acquisition that would otherwise be needed to satisfy specific absorption rate constraints.

Implication for Patient Care

- Incorporation of variable flip angles and full-Fourier acquisition into SSFSE imaging allows acquisition of pelvic images with improved image quality in less time than conventional SSFSE imaging at 3 T.

Table 1

Imaging Parameters

Parameter	Sagittal Imaging		Coronal Oblique Imaging	
	Conventional SSFSE Imaging	vrfSSFSE Imaging	Conventional SSFSE Imaging	vrfSSFSE Imaging
Refocusing flip angles (degrees)	130	$\alpha_{init} = 130$, $\alpha_{min} = 60$, $\alpha_{cent} = 100$, $\alpha_{last} = 45$	130	$\alpha_{init} = 130$, $\alpha_{min} = 60$, $\alpha_{cent} = 100$, $\alpha_{last} = 45$
Bandwidth (kHz)	±125	±125	±125	±125
Matrix	416 × 224	416 × 224	416 × 224	416 × 224
Frequency field of view (cm)	24–38	24–38	28–42	28–42
Phase field of view (%)	60–100	60–100	85–100	85–100
No. of sections acquired	30–62 (mean, 48)	30–62 (mean, 48)	30–65 (mean, 42)	30–65 (mean, 42)
Section thickness (mm)	5	5	4	4
Acceleration factor	2	2	3	3
k-space coverage	Half	Full	Half	Full
Echo time (msec)	117–125 (mean, 120)	101–186 (mean, 136)	119–129 (mean, 125)	108–158 (mean, 138)
Repetition time (msec)	1073–1695 (mean, 1358)	446–753 (mean, 613)	1204–1874 (mean, 1494)	538–771 (mean, 621)
Total sequence time (sec)	41–97 (mean, 64)	19–42 (mean, 29)	42–83 (mean, 62)	18–36 (mean, 26)
Echo spacing (msec)	5.1	4.8	5.1	4.8
Representative values from volunteer				
Echo train duration (msec)	396	511	350	427
Repetition time (msec)	1195	572	1069	491
No. of phase lines acquired	61	102	52	87

Note.—Representative values are presented for the specific case of the volunteer (a woman weighing 50 kg); echo train durations and number of phase lines acquired are dependent on the phase field of view (in this case, 80% for sagittal acquisitions and 100% for coronal oblique acquisitions) and the acceleration factor (two for sagittal acquisitions and three for coronal oblique acquisitions), while repetition times are limited by SAR, an effect that is stronger in patients who weigh less.

this approach, four control angles (initial flip angle [α_{init}], minimum flip angle reached early in the echo train [α_{min}], flip angle when the center of k-space is acquired [α_{cent}], and flip angle at the end of the echo train [α_{last}]) are used for specifying the refocusing flip angle train, with smooth modulation between these parameters. The flip angle parameters were selected semiempirically via a combination of prior simulation and clinical studies (13) and verification in a female volunteer (35 years old, with a weight of 50 kg). The flip angle parameters for vrfSSFSE imaging were chosen as follows: α_{init}, 130°; α_{min}, 60°; α_{cent}, 100°; and α_{last}, 45°. Full-Fourier acquisition was performed with linear ordering of phase encodes. A contrast-equivalent echo time (TE_{eff}) was calculated on the basis of the method of Busse et al (14) to account for the mixing of stimulated and spin echoes and resultant effective prolongation of T2 decay. TE_{eff} was set as low as possible for vrfSSFSE imaging (range, 101–186 msec; mean, 136 msec). A half-sinc RF pulse was used in which the side lobes of the RF pulse were removed to decrease the RF transmission time (15) to allow shorter effective echo times via reduced echo spacing. Additional imaging parameters are shown in Table 1.

Clinical Testing

Clinical testing was performed with institutional review board approval and informed consent. Adult patients referred for MR imaging examination of either known or suspected uterine leiomyomas were prospectively recruited and underwent imaging with a 3.0-T MR imaging unit (MR750; GE Healthcare, Waukesha, Wis) by using a 32-channel torso coil. SAR limitations were 4 W per kilogram of body weight averaged over 6 minutes and 8 W per kilogram of body weight averaged over 10 seconds. Autocalibrating reconstruction for Cartesian imaging parallel imaging was used with a parallel imaging factor of two or three for sagittal or coronal oblique acquisitions, respectively. A total of 54 consecutive female patients were included in the study between April 23, 2014, and December 31, 2014; the age range was 24–71 years (mean, 43 years), the weight range was 47–113 kg (mean, 70 kg), and there were no exclusion criteria beyond those for routine clinical MR imaging. Each subject underwent imaging with conventional SSFSE imaging (constant refocusing flip angle of 130°, half-Fourier acquisition) and vrfSSFSE imaging (variable refocusing flip angle, full-Fourier acquisition, half-sinc refocusing pulses), with all other parameters kept identical. Acquisitions were performed with the subject free breathing. Field of view was optimized for each patient's anatomy (frequency direction field of view of 24–42 cm, phase direction field of view of 60%–100%) but was identical between each pair of pulse sequences for a given subject.

Image Grading

A semiquantitative grading system based on predetermined criteria was

Table 2

Semiquantitative Scoring Criteria Used for Conventional SSFSE versus vrfSSFSE Image Evaluation

	SSFSE Imaging Favored			vrfSSFSE Imaging Favored	
Parameter	Score of −2	Score of −1	Score 0	Score of 1	Score of 2
Noise	SSFSE imaging with decreased graininess and improved diagnostic capability	SSFSE imaging with decreased graininess but without diagnostic effect	Equivalent	vrfSSFSE imaging with decreased graininess but without diagnostic effect	vrfSSFSE imaging with decreased graininess and improved diagnostic capability
Image contrast	SSFSE imaging with good image contrast between leiomyomas and myometrium; and junctional zone and myometrium not seen on vrfSSFSE images	SSFSE imaging with good image contrast between leiomyomas and myometrium; or junctional zone and myometrium not seen on vrfSSFSE images	Equivalent	vrfSSFSE imaging with good image contrast between leiomyomas and myometrium; or junctional zone and myometrium not seen on SSFSE images	vrfSSFSE imaging with good image contrast between leiomyomas and myometrium; and junctional zone and myometrium not seen on SSFSE images
Sharpness	SSFSE imaging with increased sharpness between leiomyomas and myometrium; and junctional zone and myometrium not seen on vrfSSFSE images	SSFSE imaging with increased sharpness between leiomyomas and myometrium; or junctional zone and myometrium not seen on vrfSSFSE images	Equivalent	vrfSSFSE imaging with increased sharpness between leiomyomas and myometrium; or junctional zone and myometrium not seen on SSFSE images	vrfSSFSE imaging with increased sharpness between leiomyomas and myometrium; and junctional zone and myometrium not seen on SSFSE images
Artifacts (including motion-related nonuniformity)	SSFSE imaging with decreased artifacts to the point of improved diagnostic capability	SSFSE imaging with decreased artifacts but without diagnostic effect	Equivalent	vrfSSFSE imaging with decreased artifacts but without diagnostic effect	vrfSSFSE imaging with decreased artifacts to the point of improved diagnostic capability
Ability to evaluate endometrium and cervical canal, junctional zone and cervical stroma, leiomyomas or other myometrial pathologic abnormalities, ovaries and adnexa, and musculoskeletal structures	SSFSE imaging with improved visualization to the point of improved diagnostic capability	SSFSE imaging with improved visualization but without diagnostic effect	Equivalent	vrfSSFSE imaging with improved visualization but without diagnostic effect	vrfSSFSE imaging with improved visualization to the point of improved diagnostic capability

used to compare the pulse sequences on a scale from −2 to 2 (Table 2). Subjective image quality parameters assessed were noise, image contrast, sharpness, and artifacts (including motion). Also subjectively assessed was the perceived ability to diagnostically evaluate the endometrial canal and cervical canal, the junctional zone and cervical stroma, the myometrium and leiomyomas, the ovaries and adnexa, and the musculoskeletal structures. Two readers (S.S.V. and A.M.L., with 9 and 2 years of experience in body MR image interpretation, respectively) were presented with each pair of image sequences (conventional SSFSE and vrfSSFSE image sequences) and were blinded to which image sequence was presented on the left or right (display side was randomly assigned). The grading scores were then assigned by the readers by comparing left to right, with a nonblinded assistant recording the scores and transposing them when the SSFSE image sequence was shown on the right.

Statistical Analysis

The null hypothesis of no significant difference in image quality between pulse sequences was assessed with a Wilcoxon signed rank test, with a two-tailed P value of less than .05 considered to indicate a significant difference after Holm-Bonferroni correction for multiple comparisons (16). The Wilcoxon signed rank test requires at least six effective samples (pulse sequence comparisons scored as −2, −1, 1, or 2) to be valid. Scored parameters that had fewer than six effective samples were not evaluated for significance. Interobserver variability was assessed by using a weighted Cohen κ statistic, with the weighting being the absolute difference between the reader scores. Repetition time was used as a proxy for imaging time. Differences in repetition time and TE_{eff} were assessed with the null hypothesis of no significant difference by using a Student two-tailed paired t test, with a P value less than .05 considered to indicate a statistically significant difference.
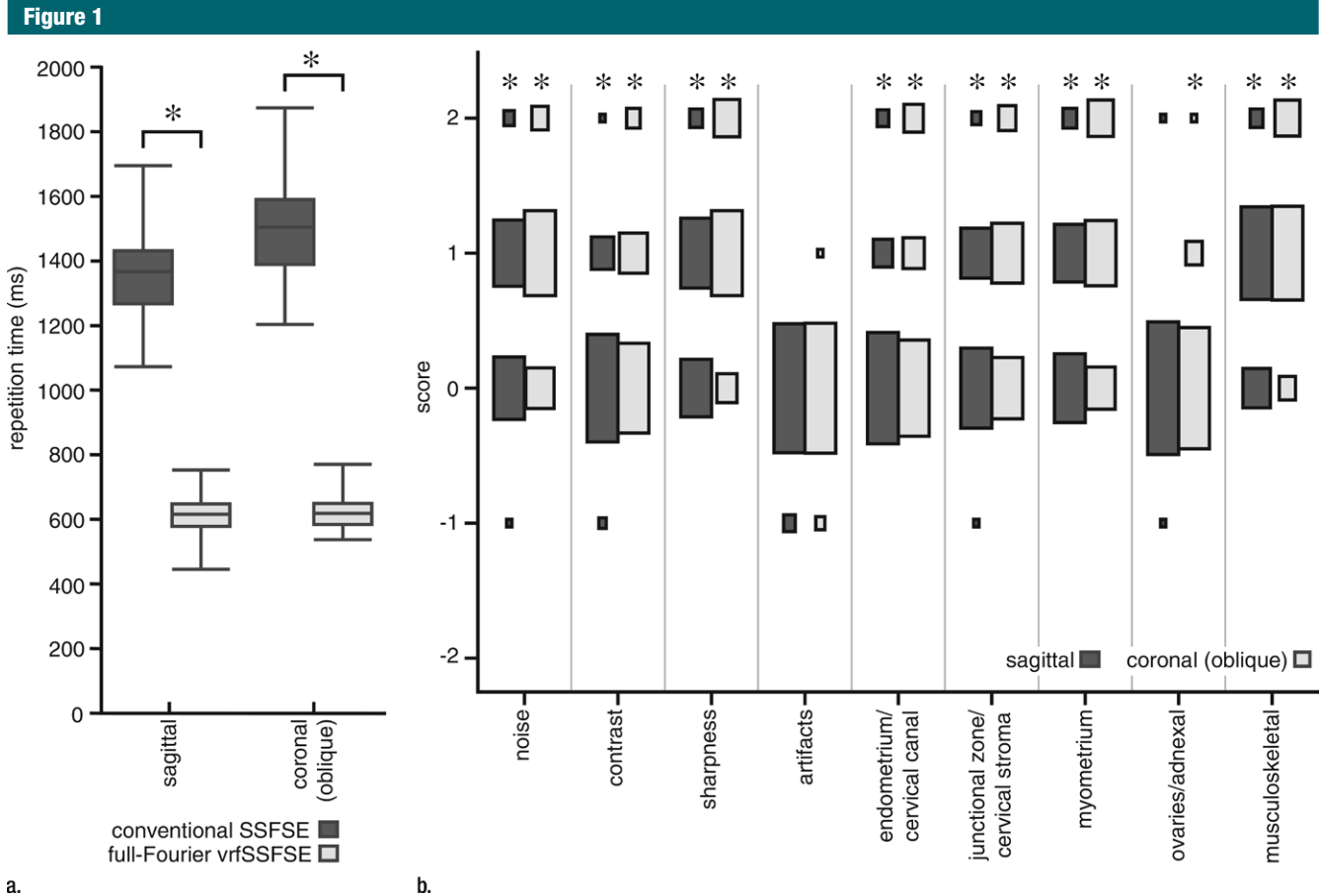
Radiology

Figure 1

Figure 1: Comparison of conventional SSFSE and vrfSSFSE imaging. **(a)** Box and whisker plot for the comparison of repetition times is shown. The box denotes the 25th–75th percentile, the middle bar denotes the median, and the top and bottom bars demonstrate the range. For each pair (conventional SSFSE vs vrfSSFSE imaging), the differences were significant ($P < .0001$). **(b)** Results of semiquantitative grading for noise, image contrast, sharpness, artifacts, and perceived ability to evaluate endometrial, myometrial, adnexal, and musculoskeletal structures and pathologic abnormalities are shown. The area of each rectangle corresponds to the relative frequency of that response. Significant P values were all less than or equal to .003, as described in the text. The scoring system used is explained in Table 2. Negative numbers favor conventional SSFSE imaging, and positive numbers favor vrfSSFSE imaging. ∗ = significant differences.

Results

Acquisition times were significantly reduced with vrfSSFSE imaging, as demonstrated by reduced repetition times (Fig 1a). For sagittal acquisitions, vrfSSFSE repetition times (mean, 613 msec) were 45% those for conventional SSFSE (mean, 1358 msec; $P < .0001$). For coronal oblique acquisitions, vrfSSFSE repetition times (mean, 621 msec) were 42% those for conventional SSFSE (mean, 1494 msec; $P < .0001$). For sagittal acquisitions, there was a significant difference ($P < .0001$) in TE_{eff} between conventional SSFSE imaging (mean TE_{eff}, 120

msec) and vrfSSFSE imaging (mean TE_{eff}, 136 msec). For coronal oblique acquisitions, there was a significant difference ($P < .0001$) in TE_{eff} between conventional SSFSE imaging (mean TE_{eff}, 125 msec) and vrfSSFSE imaging (mean TE_{eff}, 138 msec).

For sagittal acquisitions (Fig 1b), there were significant improvements for vrfSSFSE imaging in the assessed imaging quality parameters of noise (mean score, 0.56; $P < .0001$), image contrast (mean score, 0.18; $P = .0007$), and sharpness (mean score, 0.63; $P < .0001$). For coronal oblique acquisitions, there were significant improvements for vrfSSFSE imaging in

the assessed imaging quality parameters of noise, image contrast, and sharpness (mean scores of 0.81, 0.40, and 1.09, respectively; all P values < .0001). For both coronal oblique and sagittal acquisitions, the artifacts parameter had an insufficient number of differing scores (comparisons scored as other than 0) between the two pulse sequences to allow evaluation for significance.

For sagittal acquisitions (Fig 1b), the assessment of perceived diagnostic capability demonstrated significant improvements for vrfSSFSE imaging in evaluating the endometrial canal and cervical canal (mean score, 0.22;
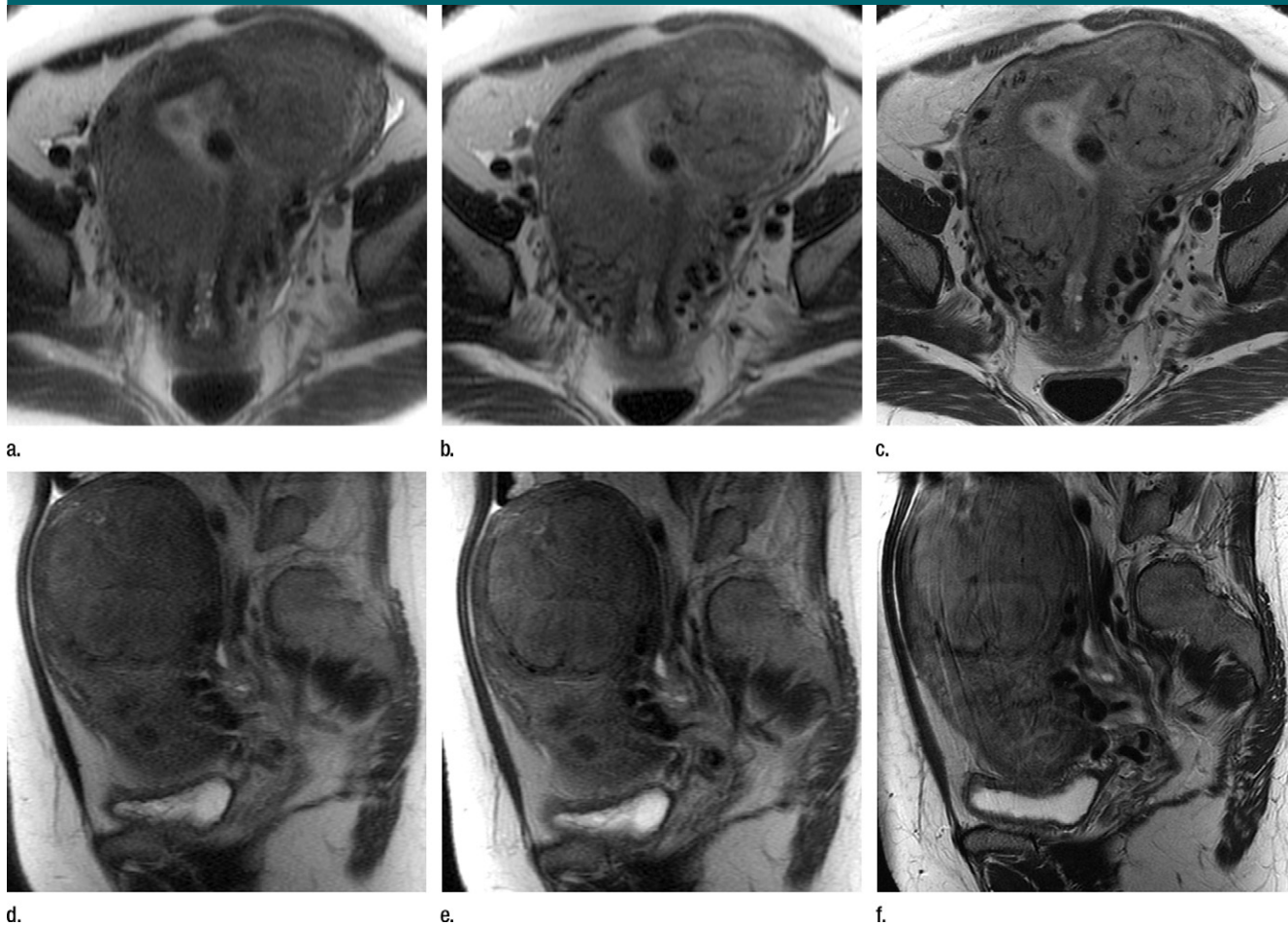
Radiology

Figure 2

Figure 2: **(a–c)** Coronal oblique and **(d–f)** sagittal T2-weighted MR images obtained in a 55-year-old woman with a large, pathologically proven intramural leiomyoma demonstrate atypical intermediate signal intensity by using conventional SSFSE **(a, d)**, vrfSSFSE **(b, e)**, and FSE **(c, f)** imaging. A small, typically appearing intramural leiomyoma is medially adjacent, and an additional, atypically appearing intramural leiomyoma along the right uterine wall is partially included in the plane of imaging. Images were cropped to 20 cm; the SSFSE and vrfSSFSE images were acquired with a 42-cm (coronal oblique) or 30-cm (sagittal) field of view, and the FSE images were acquired with a 22-cm field of view. Note the improved black-blood appearance in vessels with vrfSSFSE imaging compared with conventional SSFSE imaging, owing to its increased sensitivity to flow-related signal loss. Artifacts on the FSE images that are projecting over the uterus are from respiratory motion.

$P = .0001$), the junctional zone and cervical stroma (mean score, 0.42; $P < .0001$), the myometrium and leiomyomas (mean score, 0.56; $P < .0001$), and the musculoskeletal structures (mean score, 0.80; $P < .0001$). For evaluation of ovaries and adnexal structures on sagittal images, there was an insufficient number of differing scores (comparisons scored as other than 0) between the two pulse sequences to allow evaluation for significance. For coronal oblique acquisitions (Fig 1b), the assessment of perceived diagnostic capability demonstrated significant

improvements for vrfSSFSE imaging in evaluating the endometrial canal and cervical canal (mean score, 0.42; $P < .0001$), the junctional zone and cervical stroma (mean score, 0.65; $P < .0001$), the myometrium and leiomyomas (mean score, 0.93; $P < .0001$), the ovaries and adnexa (mean score, 0.11; $P = .003$), and the musculoskeletal structures (mean score, 1.12; $P < .0001$). The improvements for vrfSSFSE imaging were most manifest in structures with relatively short T2 relaxation times (Fig E1 [online]), such as myometrium and leiomyomas,

muscle, and bone, and were less apparent in structures with relatively long T2 relaxation times, such as endometrium and ovaries. Additional representative examples of image quality differences are shown in Figure E2 (online) and Figure 2.

The degree of improvement for both perceived image quality and perceived diagnostic capability assessments was significantly greater for the coronal oblique acquisitions than for the sagittal acquisitions (Wilcoxon signed rank test, $P = .008$). The weighted Cohen κ statistic for all observations in the

comparison of conventional SSFSE imaging versus vrfSSFSE imaging was 0.44, indicating moderate agreement between the two readers (17).

Discussion

Performing multiple orthogonal planes of T2-weighted imaging is at the core of most pelvic MR imaging protocols. Traditionally, this has been accomplished by using FSE imaging, with associated long acquisition times and lack of robustness to motion artifacts. While SSFSE imaging greatly decreases total imaging time compared with FSE imaging and brings robustness to motion artifacts from breathing and bowel peristalsis, this comes at the cost of decreased signal-to-noise ratio and image blurring arising from the extended echo train. To assess whether the limitations of SSFSE imaging could be improved on, we tested a vrfSSFSE pulse sequence in the clinical context of patients known to have or suspected of having uterine leiomyomas.

Most of the perceived imaging quality and perceived diagnostic capability parameters demonstrated significant improvements with vrfSSFSE imaging. As might be expected from the T2 decay prolongation and the full-Fourier technique used with vrfSSFSE imaging, improvements were most apparent for structures with relatively short T2 times (myometrium and leiomyomas, muscle, and bone). Improvements with vrfSSFSE imaging were greater for coronal oblique acquisitions than for sagittal acquisitions; this was believed to reflect a larger relative improvement in signal-to-noise ratio for the full-Fourier technique when used with higher acceleration factors (autocalibrating reconstruction for Cartesian imaging parallel imaging factor of three for coronal oblique acquisitions vs two for sagittal acquisitions).

Conventional SSFSE imaging is often constrained at 3 T by the RF energy deposition from the constant refocusing pulses, with dead time during multisection acquisitions added to remain within regulatory SAR constraints. Despite

the longer echo train durations used in vrfSSFSE imaging, acquisition times were reduced by more than 50% when compared with conventional SSFSE imaging, reflecting the large decrease in SAR from the reduced flip angles used in vrfSSFSE imaging.

Of the refocusing flip angle parameters (α_{init}, α_{min}, α_{cent}, and α_{last}), image quality is known to be most dependent on α_{min}; in addition to reducing SAR, lowering α_{min} leads to relative prolongation of T2 decay, and the resultant stabilization of signal over the echo train should reduce blurring (13). However, lower flip angles lead to a greater dependence on longer refocusing pathways in the echo train, creating longer time periods over which phase shifts from motion can accumulate and result in signal loss (18). This increased sensitivity to motion-related signal loss has previously been demonstrated to be of potentially limiting effect in imaging structures in close proximity to the heart, such as the left lobe of the liver when α_{min} is set to 90° (19) and the pancreas when α_{min} is set to 60° (13). In this study, no increased propensity for imaging artifacts was seen for vrfSSFSE imaging with α_{min} set to 60°, despite the free-breathing nature of the imaging acquisition, which indicates that with the refocusing flip angle parameters chosen, sufficient motion robustness is maintained for imaging structures in the pelvis.

There was a small but significant difference in effective echo time between the conventional SSFSE and vrfSSFSE pulse sequences used in this study, owing to vrfSSFSE imaging not being able to consistently achieve the target echo time (120 msec). Since the vrfSSFSE sequence is used to acquire the full k-space data in a linear fashion, acquiring additional lines in the phase-encoding direction prolongs the minimum time between the excitation pulse and when the center of k-space is acquired. Half-sinc refocusing pulses and high-bandwidth acquisition were used to decrease this minimum time, but if too many phase-encoding lines are prescribed, it is possible for this minimum time to be longer than

that required for the target echo time. The variability in echo times seen with vrfSSFSE imaging in this study was largely due to the MR imaging technologists varying the phase-direction field of view and thereby changing the number of lines acquired in the phase-encoding direction. This interdependence likewise implies that increasing the resolution in the phase-encoding direction for a fixed field of view, which also increases the number of phase-encoding lines, will necessarily prolong the minimally achievable echo time. We are currently exploring options to achieve a more consistent echo time with vrfSSFSE imaging in the pelvis, including further decreases in the α_{min} parameter to generate greater effective T2 decay prolongation and the use of outer volume suppression to reduce the number of phase encodes acquired. Even with longer effective echo times, vrfSSFSE imaging was still judged to have decreased noise when compared with conventional SSFSE imaging.

This work has several limitations. First, in this study, we only evaluated vrfSSFSE imaging in the context of pelvic MR imaging for a single indication (evaluation of leiomyomas), and we did not evaluate the utility of vrfSSFSE imaging for other common pelvic MR imaging indications. Second, the comparison in this study was performed between conventional SSFSE and vrfSSFSE imaging, as vrfSSFSE imaging is being posited as a replacement for situations where conventional SSFSE imaging is already being used. In terms of shortening pelvic MR imaging examination times, a more effective but also a more difficult comparison would be to evaluate the tradeoffs between vrfSSFSE and FSE imaging. Third, both readers practice at an institution at which both SSFSE and vrfSSFSE imaging are used. Although they were blinded to the image acquisition technique in the image analysis, the image quality differences between the pulse sequences were sufficient to allow the readers to potentially perceive which images were generated with which pulse sequence, leading to unconscious biases. Fourth,

interobserver agreement was only moderate, which likely reflects in part the subjective nature of the scoring system used. Finally, although image evaluation was performed by radiologists and included metrics to assess perceived diagnostic capability, in this study, we did not measure differences in final radiologic interpretation of the images or clinical outcomes.

In conclusion, use of a vrfSSFSE sequence leads to a doubling in acquisition speed at 3 T via reduced RF energy deposition and demonstrates significant improvements in perceived image quality and perceived diagnostic capability when evaluating structures in the pelvis.

References

1. Kaur H, Choi H, You YN, et al. MR imaging for preoperative evaluation of primary rectal cancer: practical considerations. RadioGraphics 2012;32(2):389–409.

2. Siddiqui N, Nikolaidis P, Hammond N, Miller FH. Uterine artery embolization: pre- and post-procedural evaluation using magnetic resonance imaging. Abdom Imaging 2013;38(5):1161–1177.

3. Bazot M, Stivalet A, Daraï E, Coudray C, Thomassin-Naggara I, Poncelet E. Comparison of 3D and 2D FSE T2-weighted MRI in the diagnosis of deep pelvic endometriosis: preliminary results. Clin Radiol 2013;68(1):47–54.

4. Sala E, Wakely S, Senior E, Lomas D. MRI of malignant neoplasms of the uterine corpus and cervix. AJR Am J Roentgenol 2007;188(6):1577–1587.

5. Semelka RC, Kelekis NL, Thomasson D, Brown MA, Laub GA. HASTE MR imaging: description of technique and preliminary results in the abdomen. J Magn Reson Imaging 1996;6(4):698–699.

6. Bhosale P, Ma J, Choi H. Utility of the FIESTA pulse sequence in body oncologic imaging: review. AJR Am J Roentgenol 2009;192(6 Suppl):S83–S93; Quiz S94–S97).

7. Mugler JP 3rd, Kiefer B, Brookeman JR. Three-dimensional T2-weighted imaging of the brain using very long spin-echo trains [abstr]. In: Proceedings of the Eighth Meeting of the International Society for Magnetic Resonance in Medicine. Berkeley, Calif: International Society for Magnetic Resonance in Medicine, 2000; 687.

8. Hennig J, Weigel M, Scheffler K. Multi-echo sequences with variable refocusing flip angles: optimization of signal behavior using smooth transitions between pseudo steady states (TRAPS). Magn Reson Med 2003;49(3):527–535.

9. Lichy MP, Wietek BM, Mugler JP 3rd, et al. Magnetic resonance imaging of the body trunk using a single-slab, 3-dimensional, T2-weighted turbo-spin-echo sequence with high sampling efficiency (SPACE) for high spatial resolution imaging: initial clinical experiences. Invest Radiol 2005;40(12):754–760.

10. Lebel RM, Wilman AH. Intuitive design guidelines for fast spin echo imaging with variable flip angle echo trains. Magn Reson Med 2007;57(5):972–975.

11. Busse RF, Brau AC, Vu A, et al. Effects of refocusing flip angle modulation and view ordering in 3D fast spin echo. Magn Reson Med 2008;60(3):640–649.

12. Mugler JP 3rd. Optimized three-dimensional fast-spin-echo MRI. J Magn Reson Imaging 2014;39(4):745–767.

13. Loening AM, Saranathan M, Ruangwattanapaisarn N, Litwiller DV, Shimakawa A, Vasanawala SS. Increased speed and image quality in single-shot fast spin echo imaging via variable refocusing flip angles. J Magn Reson Imaging 2015;42(6):1747–1758.

14. Busse RF, Hariharan H, Vu A, Brittain JH. Fast spin echo sequences with very long echo trains: design of variable refocusing flip angle schedules and generation of clinical T2 contrast. Magn Reson Med 2006;55(5):1030–1037.

15. Bernstein MA. Radiofrequency pulse shapes. In: Bernstein MA, King KF, Zhou XJ, eds. Handbook of MRI pulse sequences. Burlington, Mass: Elsevier Academic Press, 2004; 37–43.

16. Holm S. A simple sequentially rejective multiple test procedure. Scand J Stat 1979;6(2):65–70.

17. Landis JR, Koch GG. The measurement of observer agreement for categorical data. Biometrics 1977;33(1):159–174.

18. Litwiller DV, Holmes JH, Saranathan M, et al. Sensitivity of modulated refocusing flip angle single-shot fast spin echo to impulsive cardiac-like motion [abstr]. In: Proceedings of the Twenty-Second Meeting of the International Society for Magnetic Resonance in Medicine. Berkeley, Calif: International Society for Magnetic Resonance in Medicine, 2014; 1613.

19. Ruangwattanapaisarn N, Loening AM, Saranathan M, Litwiller DV, Vasanawala SS. Faster pediatric 3-T abdominal magnetic resonance imaging: comparison between conventional and variable refocusing flip-angle single-shot fast spin-echo sequences. Pediatr Radiol 2015;45(6):847–854.